



**HAL**  
open science

## Dynamics of PAHs and derived organic compounds in a soil-plant mesocosm spiked with $^{13}\text{C}$ -phenanthrene

Johanne Cennerazzo, Alexis de Junet, Jean-Nicolas Audinot, Corinne Leyval

### ► To cite this version:

Johanne Cennerazzo, Alexis de Junet, Jean-Nicolas Audinot, Corinne Leyval. Dynamics of PAHs and derived organic compounds in a soil-plant mesocosm spiked with  $^{13}\text{C}$ -phenanthrene. *Chemosphere*, 2016, 168, pp.1619-1627. 10.1016/j.chemosphere.2016.11.145 . hal-01417924

**HAL Id: hal-01417924**

**<https://hal.univ-lorraine.fr/hal-01417924v1>**

Submitted on 29 Aug 2019

**HAL** is a multi-disciplinary open access archive for the deposit and dissemination of scientific research documents, whether they are published or not. The documents may come from teaching and research institutions in France or abroad, or from public or private research centers.

L'archive ouverte pluridisciplinaire **HAL**, est destinée au dépôt et à la diffusion de documents scientifiques de niveau recherche, publiés ou non, émanant des établissements d'enseignement et de recherche français ou étrangers, des laboratoires publics ou privés.

1 **Dynamics of PAHs and derived organic compounds in a soil-plant**  
2 **mesocosm spiked with <sup>13</sup>C-phenanthrene.**

3

4 Johanne Cennerazzo<sup>a,b</sup>, Alexis de Junet<sup>a,b</sup>, Jean-Nicolas Audinot<sup>c</sup>, Corinne Leyval<sup>a,b</sup>

5

6 *<sup>a</sup>Université de Lorraine, Laboratoire Interdisciplinaire des Environnements Continentaux, UMR 7360,*  
7 *Vandœuvre-lès-Nancy, F-54506, France*

8 *<sup>b</sup>CNRS, Laboratoire Interdisciplinaire des Environnements Continentaux, UMR 7360, Vandœuvre-lès-Nancy, F-*  
9 *54506, France*

10 *<sup>c</sup> Advanced Instrumentation for Ion Nano-Analytics, Materials Research and Technology Department,*  
11 *Luxembourg Institute of Science and Technology, 41 rue du Brill , L-4422, Luxembourg*

12

13

14 **Abstract**

15 Polycyclic Aromatic Hydrocarbons (PAHs) are ubiquitous and persistent soil pollutants.  
16 Their fate and the influence of the plant rhizosphere on their dynamics has been extensively  
17 studied, but studies mainly focused on their dissipation rate. We conducted a plant-soil  
18 mesocosm experiment to study the fate and distribution of PAHs or derived compounds in the  
19 extractable fraction, the residual soil, the shoot biomass and the root biomass. The experiment  
20 was conducted for 21 days using ryegrass and a forest soil spiked with <sup>13</sup>C-labeled phenanthrene  
21 (PHE), using combined IRMS and NanoSIMS for analyses. Almost 90% of the initial  
22 extractable PHE content was dissipated within 3 weeks, but no rhizospheric effect was  
23 highlighted on PHE dissipation. More than 40% of <sup>13</sup>C-PHE was still in the soil at the end of  
24 the experiment, but not as PHE or PAH-derived compounds. Therefore it was under the form  
25 of new compounds (metabolites) and/or had been incorporated into the microbial biomass.

26 About 0.36% of the initial  $^{13}\text{C}$ -PHE was recovered in the root and shoot tissues, representing  
27 similar  $^{13}\text{C}$  enrichment ( $E^{13}\text{C}$ ) as in the soil ( $E^{13}\text{C} \approx 0.04$  at.%). Using NanoSIMS,  $^{13}\text{C}$  was also  
28 localized at the microscale in the roots and their close environment. Global  $^{13}\text{C}$  enrichment  
29 confirmed the results obtained by IRMS. Some hotspots of  $^{13}\text{C}$  enrichment were found, with a  
30 high  $^{32}\text{S}/^{12}\text{C}^{14}\text{N}$  ratio. Comparing the ratios, sizes and shapes of these hotspots suggested that  
31 they could be bacteria.

32

33 **Keywords:** Polycyclic Aromatic Hydrocarbons;  $^{13}\text{C}$ -Phenanthrene; soil; rhizosphere; IRMS;  
34 NanoSIMS

35

36 **Highlights:**

- 37 ➤ A mesocosm experiment with  $^{13}\text{C}$ -PHE-spiked soil was analyzed by IRMS and  
38 NanoSIMS
- 39 ➤ 40% of  $^{13}\text{C}$ -PHE was still in the soil after 21 days but not as the parent compound
- 40 ➤ Bacterium-like  $^{13}\text{C}$ -enriched hotspots were revealed by NanoSIMS close to the roots

41

## 42 1. Introduction

43 Polycyclic Aromatic Hydrocarbons (PAHs) are ubiquitous and persistent organic  
44 compounds found in the soils of large brownfield areas in many former industrial regions. They  
45 are composed of two or more benzene rings and result from the incomplete combustion by  
46 pyrolysis of organic materials from natural or anthropogenic sources (Edwards, 1983). They  
47 are persistent in soils due to their low water solubility and high adsorption on soil constituents  
48 (Wilson and Jones, 1993). They are harmful to human and environmental health, and 16 of  
49 them are listed as priority pollutants by the USEPA (Hartmann, 1996).

50 Many studies have addressed the fate and dynamics of PAHs in soils, where they can  
51 undergo numerous processes such as plant uptake, stabilization by sorption on organic and  
52 mineral phases, or transformation and degradation until total mineralization. Sorption and  
53 degradation are key processes in the fate of PAHs in the environment (Magee et al., 1991). The  
54 persistence of organic pollutants in soils has been attributed to sequestration mechanisms  
55 including intra-organic matter and intra-particle diffusion of the parent compound and  
56 transformation products (Doick et al., 2005). Plants seem to have a limited direct impact on  
57 PAH dynamics in polluted soils (Fang et al., 2001; Günther et al., 1996; Rezek et al., 2008).  
58 Gao and Zhu (2004) showed that uptake of phenanthrene and pyrene by plants accounted for  
59 less than 0.01 and 0.23% of enhanced loss in vegetated versus non-vegetated soils. The low  
60 water solubility of PAHs could prevent significant uptake by plant tissues (Binet et al., 2000;  
61 Kipopoulou et al., 1999) and root-to-shoot translocation (Burken and Schnoor, 1998). However,  
62 the indirect role of plants in PAH dynamics through their root systems is largely documented  
63 (Rezek et al., 2008; Miya and Firestone, 2000; Liste and Alexander, 2000). The plant  
64 rhizosphere is a favorable environment for high microbial diversity and activity, which permit  
65 higher PAH dissipation in soils (Corgié et al., 2003; Anderson et al., 1993; Schwab, 1994;  
66 Reilley et al. 1996). The main mechanisms involved in PAH dissipation in the soil and the  
67 rhizosphere are biodegradation and biotransformation by an active microflora (Binet et al.,  
68 2000; Wilson and Jones 1993; Cerniglia, 1997). The soil heterotrophic microflora may use  
69 organic pollutants as a source of carbon (C) and energy to grow, or for co-metabolism (Hwang  
70 and Cutright, 2002). The C derived from PAHs (C-PAH) could be (i) incorporated into the  
71 microbial biomass (Kästner et al., 1999), and/or (ii) transformed into other organic compounds  
72 and thus form part of non-extractable PAHs (Richnow et al., 1998 and 1999). The newly formed  
73 organic products could be more reactive than the parent compounds and therefore bind with  
74 soil components more easily, but could also be more toxic (Sabaté et al., 2006). Cébron et al.

75 (2011) showed that 38% of the  $^{13}\text{C}$  from labeled PAH added into soil mesocosms was not  
76 extractable after 12 days. C-PAH was still present but probably not under the form of parent  
77 PAHs or extractable compounds. Some of these newly formed organic compounds may be more  
78 soluble and more mobile than parent PAHs (Sabaté et al., 2006). However, most of the studies  
79 led so far only considered the dissipation of PAHs in the soil and in the plant rhizosphere. Some  
80 studies focused on the residual and newly formed organic compounds, especially on the  
81 distribution and the dynamics of C-PAH in the soil (Doick et al., 2005; Eschenbach et al., 1998;  
82 Kästner et al., 1999; Macleod and Semple, 2003; Northcott and Jones, 2001; Richnow et al.,  
83 1998), but no in soil-plant-microflora compartments.

84 An effective and relevant way to trace carbon compounds in soil-plant ecosystems is to  
85 use  $^{13}\text{C}$  isotopic labeling. For example, Richnow et al. (2000, 1998) used [1- $^{13}\text{C}$ ]-PAH to trace  
86 the transformation of phenanthrene in a soil reactor. But it appears more relevant to monitor C-  
87 PAH using a molecule labeled on all its carbon atoms (Cébron et al., 2011). Another  
88 complementary method to trace a labeled organic compound in soils, plants or bacteria is to  
89 map isotopic distribution at a microscale through NanoSIMS analyses (high-resolution imaging  
90 Secondary Ion Mass Spectrometry) (Hoppe et al., 2013). NanoSIMS analyses can map all the  
91 elements (isotopes) of the periodic table with an ultimate lateral resolution (probe size) in the  
92 50 to 150 nm range, high sensitivity (a few ppm), and high mass resolution (Herrmann et al.,  
93 2007; Moore et al., 2012; Remusat et al., 2012; Vidal et al., 2016).

94 The objective of our study was to investigate the fate of C-PAH in planted and non-planted  
95 soil by assessing (i) the distribution of C-PAH in the extractable fraction, the residual soil, the  
96 shoot biomass and the root biomass, and (ii) the localization of C-PAH in different  
97 compartments of the soil-plant system. We conducted a mesocosm trial using ryegrass,  $^{13}\text{C}$ -  
98 phenanthrene ( $^{13}\text{C}$ -labeled on all its carbon atoms) soil spiking, and coupling isotopic analyses  
99 with NanoSIMS analyses.

## 100 2. Materials & methods

### 101 2.1. Soil-plant mesocosms

102 Planted and non-planted mesocosms were set up, with soil spiked with either unlabeled  
103  $^{12}\text{C}$ -PHE (control) or labeled  $^{13}\text{C}$ -PHE. The soil was a Calcisol, sampled at 5-35 cm depth in a  
104 temperate beech forest close to a former coking plant (49°14.163'N, 6°0.116'E, Homecourt,  
105 Lorraine region, France). The soil horizon had a  $\text{pH}_{\text{water}}$  of 7.3; it contained 48% clay, 44% silt,  
106 7% sand, had organic carbon and total nitrogen contents of 23.0 and 1.62 g  $\text{kg}^{-1}$  respectively,  
107 and a low PAH content (13.4 mg  $\text{kg}^{-1}$ ). The soil sample was air-dried, ground and sieved to 2  
108 mm, and then spiked with 300 mg PHE  $\text{kg}^{-1}$  of soil. Spiking modalities were as follows: one  
109 with unlabeled PHE ( $^{12}\text{C}$ -PHE, Sigma Aldrich >97%) and two with known  $^{13}\text{C}$ -PHE/ $^{12}\text{C}$ -PHE  
110 mixtures ( $^{13}\text{C}$ -PHE, Sigma-Aldrich Isotec Stables Isotopes, Miamisburg, Ohio, USA). The  $^{13}\text{C}$ -  
111 PHE/ $^{12}\text{C}$ -PHE ratio was 1:8 for organic carbon analyses and 1:1 for NanoSIMS analyses. A  
112 PHE-hexane solution was added to 1:10 of the total soil mass for spiking. Hexane was  
113 evaporated under a fumehood, and then the spiked soil was homogenized with the remaining  
114 9:10 of soil mass.

115 The planted and non-planted mesocosms were conducted in 50-mL glass jars with 40 g  
116 of PHE-spiked soil. They were inoculated with 10 mL of soil suspension from a PAH-  
117 contaminated soil (200 g  $\text{L}^{-1}$  in 0.85% NaCl) to ensure that a PAH-degrading microflora was  
118 present. Five ryegrass (*Lolium perenne*) seeds were added in each planted mesocosm. The  
119 experiment was conducted in a growth chamber under controlled conditions (22°C/18°C with  
120 16h/8h day/night, 250  $\mu\text{mol photons m}^{-2} \text{ s}^{-1}$ , 80% relative humidity) for 21 days. Four replicates  
121 were prepared for each planted and non-planted modality and each sampling time (0, 7, 14 and  
122 21 days), and for each  $^{12}\text{C}$ -PHE- and  $^{13}\text{C}$ -PHE/ $^{12}\text{C}$ -PHE- (1:8 ratio) spiked soil, except for 1:1  
123  $^{13}\text{C}$ -PHE/ $^{12}\text{C}$ -PHE-spiked soil (one replicate, and sampling after 7 and 14 days for NanoSIMS  
124 microprobe analyses). At each sampling time, ryegrass shoots and roots were removed from

125 the soil and separated. The roots were washed with distilled water and dried with filter paper.  
126 The fresh plant material and soil were oven-dried at 35 °C and then ground, and the soil was  
127 sieved to 200  $\mu\text{m}$  prior to analyses. The roots were prepared directly after sampling for  
128 elemental mapping analyses.

129

## 130 2.2. Organic and isotopic analyses

131 PHE was extracted from 2 g of dry soil using dichloromethane (DCM) and a high-  
132 pressure and high-temperature DIONEX® 200 ASE (Accelerated Solvent Extractor) automated  
133 extractor. Residual soil (after PAH extraction) was kept for organic analyses. DCM was  
134 evaporated from the PAH extracts under  $\text{N}_2$  flow and replaced by acetonitrile for PAH analysis.  
135 PAH extracts were analyzed using a reverse-phase chromatography UHPLC Ultimate 3000  
136 RSLC system (Dionex) equipped with a Diode Array Detector and a Zorbax Eclipse PAH  
137 RRHD column (100 mm x 2.1 mm, 1.8  $\mu\text{m}$  – Agilent). The mobile phase was a mixture of  
138 water/acetonitrile in gradient mode, with a flow rate of 0.420  $\text{mL min}^{-1}$ . The wavelength used  
139 for detection was 254 nm.

140

141 Isotopic and elemental analyses were performed on bulk and residual soil (before and  
142 after PAH extraction, respectively), and on ryegrass shoot and root biomass using EA-  
143 GC/IRMS (Elementary analyzer – Isotope Ratio Mass Spectrometry 100, IsoPrime,  
144 Manchester. EA: IsotopeCube, Elementar, Hanau). Approximately 1.0 mg of the powdered  
145 material of each sample was weighed and placed in 6x4 mm tin capsules (Elemental  
146 Microanalysis Limited, Devon, UK). Analyses were carried out at the Technical Platform of  
147 Functional Ecology (OC 081) at the INRA Forest Ecology and Eco-Physiology Unit. Isotopic  
148 measurements were reported in the delta notation ( $\delta$  expressed in ‰) as:

149 
$$\delta^{13}\text{C} (\text{‰}) = \left( \frac{R_{\text{sample}}}{R_{\text{Ref}}} - 1 \right) \times 1000$$
 Eq. 1

150 Where  $R_{\text{sample}} = {}^{13}\text{C}_{\text{sample}}/{}^{12}\text{C}_{\text{sample}}$  for labeled and control samples, and  $R_{\text{Ref}}$  refers to the Vienna  
 151 Pee Dee Belemnite (VPDB) standard, with  $R_{\text{Ref}} = {}^{13}\text{C}_{\text{PDB}}/{}^{12}\text{C}_{\text{PDB}} = 0.0112375$ .

152 Enrichment in  ${}^{13}\text{C}$  ( $E^{13}\text{C}$ ), expressed as excess ‰ of atoms (at.‰), was calculated relatively to  
 153 the unlabeled control in the soil and in the plant, as follows:

154 
$$E^{13}\text{C} (\text{at.‰}) = ({}^{13}\text{C}_{\text{labeled}} - {}^{13}\text{C}_{\text{control}})$$
 Eq. 2

155 Where  ${}^{13}\text{C}_{\text{labeled}} (\text{at.‰}) = [R_{\text{labeled}}/(R_{\text{labeled}} + 1)] \times 100$ ,  ${}^{13}\text{C}_{\text{control}} (\text{at.‰}) = [R_{\text{control}}/(R_{\text{control}} + 1)] \times 100$ .

156  $E^{13}\text{C}$  was calculated for bulk soil, residual soil, and ryegrass shoot biomass and root biomass.

157 Soil and plant  ${}^{13}\text{C}$  concentrations ( ${}^{13}\text{C}_{\text{conc}}$ ) were also calculated (expressed as  $\mu\text{g C g}^{-1}$  of soil and  
 158  $\mu\text{g C g}^{-1}$  of plant, respectively):

159 
$${}^{13}\text{C}_{\text{conc}} (\mu\text{g C g}^{-1}) = \left( \frac{{}^{13}\text{C}_{\text{initial}} - {}^{13}\text{C}_{\text{loss}}}{100} \right) \times C_x$$
 Eq. 3

160 Where  $C_x$  refers to the C content, expressed in  $\mu\text{g C g}^{-1}$  of soil or plant.  ${}^{13}\text{C}$  distribution (%) in  
 161 the mesocosms was deduced from the  ${}^{13}\text{C}$  concentrations and by considering that the percentage  
 162 of  ${}^{13}\text{C}$  initially added in the soil after PHE-spiking was 100% (T0).  ${}^{13}\text{C}$  distribution (%) was  
 163 calculated for the PAH extracts, the residual soil and the plants. The remaining  ${}^{13}\text{C}$  was  
 164 considered as  ${}^{13}\text{C}$  loss.

### 165 2.3. Elemental mapping analyses in the roots

166 The fresh ryegrass roots harvested after 7 and 14 days were rapidly cut into 0.5-cm  
 167 pieces and placed on adhesive film. The fine roots were cryofixed using a LEICA EM CPC  
 168 Universal Cryoworkstation. They were frozen at atmospheric pressure ( $10^5 \text{ °C s}^{-1}$ ), and  
 169 slammed on copper mirrors (Printz et al., 2016). Then the cryofixed samples were lyophilized  
 170 (LEICA EM CFD) without using any solvent ( $1 \text{ °C h}^{-1}$  for 8 days down to  $-20 \text{ °C}$  at  $1.10^{-4} \text{ Pa}$ )  
 171 (Printz et al., 2016). The root samples were finally embedded in Epoxy resin and coated with  
 172 gold prior to analyses by nano Secondary Ion Mass Spectrometry.

173 Elemental mapping was performed using a Cameca NanoSIMS 50 ion probe  
174 (Gennevilliers, France) in the raster-imaging mode. The probe detects the secondary ions  
175 generated from each pulverized sample surface by an energetic incident ion beam (Hoppe et  
176 al., 2013). Ion images were obtained using a beam of Cs<sup>+</sup> primary ions with an energy impact  
177 of 16 keV and a beam current of 0.8 pA on the sample. The images were recorded in 256x256  
178 pixels; under these conditions, a lateral resolution of 80-100 nm was expected. Negative  
179 secondary ion signals for <sup>12</sup>C<sup>-</sup>, <sup>13</sup>C<sup>-</sup>, <sup>12</sup>C<sup>14</sup>N<sup>-</sup>, <sup>32</sup>S<sup>-</sup> ions and <sup>12</sup>C<sup>14</sup>N<sup>-</sup>, <sup>56</sup>Fe<sup>16</sup>O<sup>-</sup> clusters (Behrens et  
180 al., 2008) were collected simultaneously using the multicollection system. Images were  
181 acquired with a counting time of 30 ms/pixel. Mass resolution (M/ΔM) was above 4500 (e.g. 2  
182 916 was required to resolve mass interference between <sup>13</sup>C and <sup>12</sup>C<sup>1</sup>H), and mass calibration  
183 was achieved using standard iron oxide references. The isotope ratio of the two <sup>12</sup>C and <sup>13</sup>C  
184 carbon isotopes allowed us to localize and quantify the <sup>13</sup>C-labeled PHE. The quantitative data  
185 acquired by NanoSIMS were calculated with Winimage software that directly processes image  
186 data (CAMECA file format) and measures the δ<sup>0</sup>/<sub>00</sub> isotopic deviation according to the δ<sup>0</sup>/<sub>00</sub>  
187 formula (Eq. 1) for each pixel. The deviation of the <sup>13</sup>C/<sup>12</sup>C ratio was calculated based on a fixed  
188 R<sub>ref</sub> value (commonly 1.107%, the natural isotope ratio for <sup>13</sup>C). The isotopic ratio of <sup>13</sup>C  
189 determined by NanoSIMS was not compare to IRMS values because of the presence of the  
190 epoxy resin which prevent a specific <sup>13</sup>C signal of organic matter (Vidal et al., 2016). The scale  
191 of all the images of isotopic map deviation was kept constant (0 to 300) to allow for a quick  
192 comparison of intensity levels.

193 Carbon-to-nitrogen (<sup>12</sup>C/<sup>12</sup>C<sup>14</sup>N) and sulfur-to-nitrogen (<sup>32</sup>S/<sup>12</sup>C<sup>14</sup>N) ratio data were extracted  
194 from regions of interest (ROIs) by using the freeware package Image J. Each ROI was drawn  
195 at least twice for each group in order to obtain a mean ratio for any given area. Linescan  
196 (=segments of variable length drawn on the ion image) data were also extracted using  
197 OpenMIMS plugging with ImageJ software. Preparation and SIMS analyses were carried out

198 with a Cameca NanoSIMS 50 at the Luxembourg Institute of Science and Technology (LIST)  
199 in Esch-sur-Alzette, Luxembourg.

200

#### 201 2.4. Statistical analyses

202 Statistical analyses were performed using R software (version 3.1.3, 2015). All tests were  
203 used with a 95% significant level. Parametric conditions were checked with Shapiro-Wilk's  
204 test for normality and with Bartlett's test for homogeneity of variance. When normality  
205 conditions were not met, a non-parametric statistical test was used for multiple comparisons of  
206 means. Two-way analysis of variance (ANOVA 2) followed by Tukey's post hoc test was used  
207 for the comparison of PHE and  $^{13}\text{C}$  concentrations between sampling times and between  
208 treatments. For NanoSIMS analysis, the relative abundance levels of  $^{13}\text{C}$  from ROI were  
209 compared with a non-parametric analysis of variance (Kruskal-Wallis test).

210

### 211 3. Results

#### 212 3.1. Phenanthrene concentrations in planted and non-planted mesocosms

213 The extractable PHE concentration immediately after soil spiking (T0) was  $171.6 \pm 0.7$   
214  $\text{mg kg}^{-1}$  (Figure 1). After 7 days, PHE concentrations were  $128.1 \pm 9.7$  and  $137.6 \pm 10.8$   $\text{mg kg}^{-1}$   
215 in the planted and non-planted mesocosms, respectively, indicating 20-25% PHE dissipation.  
216 The main decrease in PHE concentration was noted after 14 days, with  $49.8 \pm 15.6$  and  $40.2 \pm$   
217  $15.9$   $\text{mg kg}^{-1}$  of PHE in the planted and non-planted mesocosms, respectively, i.e.  
218 approximately 70% of PHE loss. Finally, after 21 days there remained less than  $20$   $\text{mg kg}^{-1}$  of  
219 PHE in each mesocosm. The PHE concentration decreased significantly over time: 90% of the

220 added PHE was dissipated after 21 days. No significant difference in PHE concentrations was  
221 noted over time between the planted and non-planted mesocosms.

222

### 223 3.2. $^{13}\text{C}$ -enrichment and distribution in the planted and non-planted mesocosms

224  $^{13}\text{C}$ -enrichment ( $E^{13}\text{C}$ ) values are summarized in Table 1 and Figure 2a. No significant  
225 difference in  $E^{13}\text{C}$  was noted between the planted and non-planted mesocosms.  $E^{13}\text{C}$  of the bulk  
226 soil decreased from 0.097 at.% at T0 down to 0.047 at.% after 21 days, while  $E^{13}\text{C}$  of the  
227 residual soil increased from 0.005 at.% to 0.044 at.% over the same time period. At the end of  
228 the trial, there was no significant difference in  $^{13}\text{C}$  concentration between the bulk and residual  
229 soils, indicating that  $^{13}\text{C}$  was mainly present in the residual soil under a non-extractable form  
230 (Table 1).  $E^{13}\text{C}$  in plant tissues was studied after 7 days. It reached 0.015 at.% and 0.017 at.%  
231 in the roots and shoots, respectively. From 14 days, no significant difference was noted between  
232 root and shoot  $E^{13}\text{C}$  due to the high heterogeneity of values. After 21 days,  $E^{13}\text{C}$  in residual soil  
233 as well as in ryegrass shoots and roots was around 0.04 at.%.

234  $^{13}\text{C}$  distribution was measured over time for the different compartments of the  
235 mesocosms: residual soil, PAH extract, plant, and C loss (Figure 2b). At T0, 94% of the total  
236  $^{13}\text{C}$  content was recovered in the PAH extract, and 6% in the residual soil. The  $^{13}\text{C}$  content of  
237 the PAH extract decreased over time down to 3-11% of the total  $^{13}\text{C}$  content, while it increased  
238 significantly in residual soil and reached 45-48% of the total  $^{13}\text{C}$  content after 21 days. The  
239 ryegrass  $^{13}\text{C}$  content represented less than 1% of the total  $^{13}\text{C}$  content, mainly due to the very  
240 low dry mass as compared to the total mass of soil (a few mg versus 40 g). The  $^{13}\text{C}$  loss from  
241 mesocosms accounted for 19% after 7 days and up to 43% after 14 days.

242

243 3.3. Mapping of  $^{13}\text{C}$  enrichment in ryegrass roots

244 NanoSIMS analyses were carried out on unlabeled and labeled roots after 7 and 14 days.  
245 The mean percentages of  $^{13}\text{C}$  atoms in the roots were 1.09 in unlabeled (control) roots, 1.11 in  
246  $^{13}\text{C}$ -labeled roots after 7 days, and 1.15 in  $^{13}\text{C}$ -labeled roots after 14 days. A significant  $^{13}\text{C}$ -  
247 enrichment was noted in labeled roots after 14 days relatively to the control.

248 A mapping of  $^{13}\text{C}$  associated with  $^{12}\text{C}$ ,  $^{12}\text{C}^{14}\text{N}$ ,  $^{32}\text{S}$ ,  $^{56}\text{Fe}^{16}\text{O}$  ion species was performed on  
249 root cross sections after 14 days (Figure 3). The roots were clearly identified in association with  
250 high  $^{12}\text{C}$ -,  $^{12}\text{C}^{14}\text{N}$ - and  $^{32}\text{S}$ - signals. The resin was clearly visible with high  $^{12}\text{C}$ - levels but no  
251  $^{12}\text{C}^{14}\text{N}$ - or  $^{32}\text{S}$ - intensity, and was easily differentiated from the root tissue. Mineral particles  
252 such as iron oxides, assimilated to soil particles, were highlighted by the  $^{56}\text{Fe}^{16}\text{O}$ - signal and  
253 they were only observed surrounding the root. The composite image resulting from the overlay  
254 of  $^{12}\text{C}$ ,  $^{12}\text{C}^{14}\text{N}$  and  $^{13}\text{C}$  elements emphasized  $^{13}\text{C}$  enrichment localization. There was no visual  
255 evidence of global  $^{13}\text{C}$  enrichment in the roots, but rather locally distributed hotspots. Three  
256 zones were identified close to the root epidermis (Figure 4), but none close to the soil particles.  
257 These hotspots were mainly oval-shaped, and 1 to 2  $\mu\text{m}$  in diameter.

258 An area of interest, pinpointed by the white square in Figure 3, was enlarged and  
259 presented in Figure 4.a) Hotspots (red), root (green and blue association), soil (white) and resin  
260 (green) were well identified. The black zone between the resin and the root could be holes that  
261 formed during sample preparation. The hotspots were adherent to the root epidermal cells but  
262 not to the soil particles. A linescan was drawn through root and hotspots (Figure 4.b) to study  
263  $^{12}\text{C}$ -,  $^{13}\text{C}$ -,  $^{12}\text{C}^{14}\text{N}$ - and  $^{32}\text{S}$ - distribution. It showed that a higher  $^{13}\text{C}$ - signal as compared to  $^{12}\text{C}$ - was  
264 correlated with a higher  $^{32}\text{S}$ - signal as compared to  $^{12}\text{C}^{14}\text{N}$ -. This higher  $^{32}\text{S}$ - signal as compared  
265 to  $^{12}\text{C}^{14}\text{N}$ - was not observed in the root but only in the hotspot, so that the hotspots appeared to  
266 be made of something else than root tissue.  $^{12}\text{C}/^{12}\text{C}^{14}\text{N}$ -,  $^{32}\text{S}/^{12}\text{C}^{14}\text{N}$  and  $^{56}\text{Fe}^{16}\text{O}/^{12}\text{C}$  ratios were  
267 also calculated for ROI selection in the hotspots, root tissue, soil particles and resin (Table 2).

268 Hotspots were easily discriminated from roots because they displayed significantly higher  
269  $^{12}\text{C}/^{13}\text{C}$  and  $^{32}\text{S}/^{34}\text{S}$  ratios. They were not considered as soil particles because they had a  
270 low  $^{56}\text{Fe}/^{54}\text{Fe}$  ratio, or as resin because they contained less C than resin ( $^{12}\text{C}/^{13}\text{C}$  ratios  
271 equivalent to 12.88 for resin and 1.02 for hotspots).

## 272 **4. Discussion**

### 273 4.1. Effect of the rhizosphere on phenanthrene degradation

274 The extractable PHE concentration decreased by 40% after spiking and by up to 90%  
275 after 21 days in the planted and non-planted systems (Figure 1). This rapid dissipation of PHE  
276 and its high rate are in part explained by experimental conditions, including the high  
277 bioavailability of the freshly spiked pollutant and soil inoculation with adapted microflora.  
278 Smith et al. (2011) showed that using a soil freshly spiked with pure PAH led to a greater loss  
279 than using historically contaminated soils. Inoculation of a microflora extracted from PAH-  
280 contaminated soil had a priming effect in the first days following contamination and increased  
281 PHE degradation (Joner et al., 2004, 2002). Low-molecular-weight PAHs such as PHE (3 rings)  
282 can be used as primary substrates and be easily broken down in the soil by adapted microflora  
283 commonly found in polluted soils (Cerniglia, 1997). This rapid PHE degradation could mask a  
284 potential rhizospheric effect, even in a forest soil. No significant difference was noted in  $^{13}\text{C}$ -  
285 dynamics between the planted and non-planted systems (Figure 2). Therefore there is no  
286 evidence of an impact of the rhizosphere on PAH degradation in this type of plant-soil  
287 mesocosm.

288

### 289 4.2. Dynamics of phenanthrene carbon in the plant-soil mesocosms

290 The dynamics of PHE degradation was studied by monitoring the increase in C loss  
291 and C incorporation in the soil (Figure 2.a). The loss of  $^{13}\text{C}$  during the first 14 days

292 represented half of the spiked  $^{13}\text{C}$  (Figure 2.b). We hypothesized that a major part of the  
293 PHE loss was mineralized as  $\text{CO}_2$ . There was no significant difference in PHE degradation  
294 between 14 and 21 days, which means that PHE degradation occurred during the first days  
295 of contamination.

296         After 14 days, almost 40% of PHE carbon had been incorporated in the soil. This result  
297 is in accordance with the 38% of  $^{13}\text{C}$  remaining in the soil after 12 days in comparable soil  
298 mesocosms used to identify PAH-degrading bacteria (Cébron et al., 2011). No PHE metabolite,  
299 like those identified by Käckler et al. (2002) and Richnow et al. (2000) for example, was  
300 detected by GC-MS analysis of PAH extracts. The remaining  $^{13}\text{C}$  incorporated in the soil must  
301 then have been present under the form of other organic compounds that were not extracted by  
302 dichloromethane. Kästner et al. (1999) conducted a long-term experiment on the transformation  
303 of  $^{13}\text{C}$ -labeled PAHs in soil bioreactors; they highlighted that the non-extractable residue had  
304 a relatively high stability over time. These organic compounds, newly formed from PAHs,  
305 become soil-bound residues (Binet et al., 2000) and/or a C source for microorganisms (Richnow  
306 et al., 1998; 2000). For Richnow et al. (1999), the formation of these compounds most probably  
307 depends on an intense microbial activity. Soil microorganisms may use organic pollutants like  
308 PAHs as a C source and transform them into biomass through anabolic processes. Part of these  
309 newly formed compounds can also be incorporated into organo-mineral complexes and be  
310 protected against degradation depending on the nature of mineral phases (de Junet et al., 2013).  
311 This could explain why these organic compounds remain non-available in the soil (Macleod  
312 and Semple, 2003; Pignatello and Xing, 1996) and have a relative high stability (Richnow et  
313 al., 1999).

314         Less than 1% of total PHE carbon was taken up by ryegrass roots and shoots. No  
315 significant difference was noted between the two plant parts after 14 and 21 days. Plant  
316  $^{13}\text{C}$  enrichment was similar to soil  $^{13}\text{C}$  enrichment, namely about 0.04 at.% (Figure 2a), and

317 the difference expressed in total amounts was only due to the difference in mass between  
318 the soil and the plants. However, according to NanoSIMS analyses (Figure 4), there was  
319 no evidence of direct PHE uptake by plant roots. A small part of PHE may have been  
320 sorbed onto the root epidermis, more precisely near the suberized exodermis and  
321 endodermis (Dupuy et al., 2016). Previous studies show preferential PAH incorporation in  
322 shoots through atmospheric deposition, and low direct incorporation by roots (Binet et al.,  
323 2000a; Desalme et al., 2011; Schwab and Banks, 1994). If  $^{13}\text{C}$  was not taken up by the  
324 roots under the form of PHE, it may have been taken up under the form of newly formed  
325 organic compounds or  $^{13}\text{C}\text{-CO}_2$ . It could be absorbed or adsorbed from ambient air by the  
326 shoots after PHE volatilization (Gao and Zhu, 2004) or through stomata under the form of  
327  $^{13}\text{C}\text{-CO}_2$  during the photosynthetic process.  $^{13}\text{C}$  enrichment was also noted in roots by SIMS,  
328 confirming the excess  $^{13}\text{C}$  recovered in the roots (Figure 2.a).

329

#### 330 4.3. Determination of $^{13}\text{C}$ hotspots and localization of $^{13}\text{C}$ in ryegrass roots

331 There was no correlation between the  $^{56}\text{Fe}^{16}\text{O}$  and  $^{13}\text{C}$  signals close to the roots after 14  
332 days, therefore SIMS analyses did not evidence any contribution of organic matter-mineral  
333 associations to the  $^{13}\text{C}$ -PAH dynamics. However two types of enrichment were highlighted  
334 in the plant rhizosphere: a global  $^{13}\text{C}$  enrichment and  $^{13}\text{C}$  hotspots. Hotspots were composed  
335 of  $^{12}\text{C}^-$ ,  $^{12}\text{C}^{14}\text{N}^-$  and  $^{32}\text{S}^-$  ions species. Sulfur and nitrogen contents suggest the presence of  
336 proteins (Eybe et al., 2008) that could originate from the plants or from microorganisms.  
337 Hotspots were discriminated from root tissues based on their high  $^{32}\text{S}$  content as compared to  
338 the roots (Figure 4 and Table 2). The  $^{32}\text{S}/^{12}\text{C}^{14}\text{N}$  ratio of the hotspots (0.11) was around five  
339 times higher than the  $^{32}\text{S}/^{12}\text{C}^{14}\text{N}$  ratio of the ryegrass roots (0.02). This last value is in  
340 accordance with the  $^{32}\text{S}/^{12}\text{C}^{14}\text{N}$  ratio of 0.027 found by Dijkshoorn and Van Wijk (1967) in  
341 ryegrass shoots. The oval shape of the hotspots and their size (1 to 2  $\mu\text{m}$  in diameter) are in

342 accordance with the shape and size of bacteria. Moreover, measurements were performed on  
343 isolated bacteria (unpublished data) and showed similar ratios (0.1 for  $^{32}\text{S}/^{12}\text{C}^{14}\text{N}$ ). There was  
344 evidence of global  $^{13}\text{C}$  enrichment during plant growth, but no PAH uptake by the roots was  
345 visualized by NanoSIMS analyses (Figure 4). The main  $^{13}\text{C}$ -PAH uptake could be attributed to  
346 the bacteria present in the rhizospheric environment.

347

## 348 **5. Conclusion**

349 A mesocosm experiment was conducted using  $^{13}\text{C}$ -phenanthrene to monitor the  
350 dynamics of PHE and derived compounds in the soil and in ryegrass. After 21 days, almost  
351 90% of spiked PHE had been degraded. PHE was mainly mineralized under gas phase (up to  
352 53%, corresponding to the  $^{13}\text{C}$  loss). But after 14 days, more than 40% of PHE carbon had been  
353 transformed into newly formed organic compounds (metabolites) or incorporated into the  
354 microbial biomass. No rhizospheric effect on PAH dynamics was noted due to the rapid  
355 dissipation of PHE. Less than 1% of PHE carbon was also found in the root and shoot tissues  
356 of ryegrass. The plant  $\text{E}^{13}\text{C}$  was similar to the soil  $\text{E}^{13}\text{C}$  ( $\sim 0.04$  at.%), suggesting a homogeneous  
357 C-PAH distribution in the plant-soil mesocosm.

358 Global root C-PAH enrichment was also determined in the ryegrass rhizosphere at a  
359 finer scale using NanoSIMS, based on  $^{13}\text{C}/^{12}\text{C}$  ratio measurements on images obtained for  
360 control ( $^{12}\text{C}$ ) and labeled samples after 7 and 14 days. There was no evidence of  $^{13}\text{C}$ -PAH  
361 association to iron oxides in the close root environment. However, hotspots of  $^{13}\text{C}$  enrichment  
362 close to the roots probably indicated the presence of bacteria, as suggested by their size, shape  
363 and element composition. A part of PAH carbon was sorbed on the roots, but it was mainly  
364 incorporated into the bacteria mentioned above. These bacteria probably degraded PHE and  
365 incorporated PHE-derived  $^{13}\text{C}$  into their biomass.

366 The use of labeled contaminants and the coupling of IRMS and NanoSIMS is a relevant  
367 and powerful tool for determining the dynamics of these contaminants. The dynamics of  $^{13}\text{C}$   
368 from labeled PAH was highlighted by  $^{13}\text{C}$ -partitioning at a global level, but the transformation  
369 of PAH  $^{13}\text{C}$  at a molecular level remains to be investigated. Complementary techniques such as  
370  $^{13}\text{C}$ -NMR and pyGCMS could be used to further characterize the  $^{13}\text{C}$ -PAH metabolites.

371

### 372 **Acknowledgements**

373 This work was supported by a grant from the University of Lorraine and the Lorraine  
374 Region. The authors thank David Billet for UHPLC analyses and Patrick Grysan for NanoSIMS  
375 analyses.

376

### 377 **References**

378 Anderson, T.A., Guthrie, E., Walton, B.T., 1993. Bioremediation in the rhizosphere. *Environ.*  
379 *Sci. Technol.* 27, 2630–2636. doi:10.1021/es00049a001

380 Behrens, S., Lösekann, T., Pett-Ridge, J., Weber, P.K., Ng, W.O., Stevenson, B.S., Hutcheon,  
381 I.D., Relman, D.A., Spormann, A.M., 2008. Linking microbial phylogeny to metabolic  
382 activity at the single-cell level by using enhanced element labeling-catalyzed reporter  
383 deposition fluorescence in situ hybridization (EL-FISH) and NanoSIMS. *Appl. Environ.*  
384 *Microbiol.* 74, 3143–3150. doi:10.1128/AEM.00191-08

385 Binet, P., Portal, J.M., Leyval, C., 2000a. Fate of polycyclic aromatic hydrocarbons (PAH) in  
386 the rhizosphere and mycorrhizosphere of ryegrass. *Plant Soil* 227, 207–213.  
387 doi:10.1023/A:1026587418611

388 Binet, P., Portal, J.M., Leyval, C., 2000b. Dissipation of 3–6-ring polycyclic aromatic  
389 hydrocarbons in the rhizosphere of ryegrass. *Soil Biol. Biochem.* 32, 2011–2017.  
390 doi:10.1016/S0038-0717(00)00100-0

391 Burken, J.G., Schnoor, J.L., 1998. Predictive relationships for uptake of organic contaminants  
392 by hybrid poplar trees. *Environ. Sci. Technol.* 32, 3379–3385. doi:10.1021/es9706817

393 Cébron, A., Louvel, B., Faure, P., France-Lanord, C., Chen, Y., Murrell, J.C., Leyval, C., 2011.  
394 Root exudates modify bacterial diversity of phenanthrene degraders in PAH-polluted soil  
395 but not phenanthrene degradation rates. *Environ. Microbiol.* 13, 722–736.  
396 doi:10.1111/j.1462-2920.2010.02376.x

397 Cerniglia, C.E., 1997. Fungal metabolism of polycyclic aromatic hydrocarbons: past, present  
398 and future applications in bioremediation. *J. Ind. Microbiol. Biotechnol.* 19, 324–33.

399 Corgié, S.C., Joner, E.J., Leyval, C., 2003. Rhizospheric degradation of phenanthrene is a  
400 function of proximity to roots. *Plant Soil* 257, 143–150. doi:10.1023/A:1026278424871

401 de Junet, A., Basile-Doelsch, I., Borschneck, D., Masion, A., Legros, S., Marol, C., Balesdent,  
402 J., Templier, J., Derenne, S., 2013. Characterisation of organic matter from organo-mineral  
403 complexes in an Andosol from Reunion Island. *J. Anal. Appl. Pyrolysis* 99, 92–100.  
404 doi:10.1016/j.jaap.2012.10.020

405 Desalme, D., Binet, P., Bernard, N., Gilbert, D., Toussaint, M.L., Chiapusio, G., 2011.  
406 Atmospheric phenanthrene transfer and effects on two grassland species and their root  
407 symbionts: a microcosm study. *Environ. Exp. Bot.* 71, 146–151.  
408 doi:10.1016/j.envexpbot.2010.11.009

409 Dijkshoorn.W., Van Wijk.L., 1967. The sulphur requirements of plants evidenced by the  
410 sulphur-nitrogen ratio in the organic matter a review of published data. *Plant Soil* 26, 129–  
411 157.

412 Doick, K.J., Burauel, P., Jones, K.C., Semple, K.T., 2005. Distribution of aged <sup>14</sup>C-PCB and  
413 <sup>14</sup>C-PAH residues in particle-size and humic fractions of an agricultural soil. *Environ.*  
414 *Sci. Technol.* 39, 6575–6583. doi:10.1021/es050523c

415 Dupuy, J., Leglize, P., Vincent, Q., Zelko, I., Mustin, C., Ouvrard, S., Sterckeman, T., 2016.

416 Effect and localization of phenanthrene in maize roots. *Chemosphere* 149, 130–136.  
417 doi:10.1016/j.chemosphere.2016.01.102

418 Edwards, N.T., 1983. Polycyclic Aromatic Hydrocarbons (PAH's) in the Terrestrial  
419 Environment - A Review. *J. Environ. Qual.* 12, 427–441.  
420 doi:10.2134/jeq1983.00472425001200040001x

421 Eschenbach, A., Wienberg, R., Mahro, B., 1998. Fate and stability of nonextractable residues  
422 of [<sup>14</sup>C] in contaminated soils under environmental stress conditions. *Environ. Sci.*  
423 *Technol.* 32, 2585–2590. doi:10.1021/es9708272

424 Eybe, T., Audinot, J.N., Bohn, T., Guignard, C., Migeon, H.N., Hoffmann, L., 2008. NanoSIMS  
425 50 elucidation of the natural element composition in structures of cyanobacteria and their  
426 exposure to halogen compounds. *J. Appl. Microbiol.* 105, 1502–1510. doi:10.1111/j.1365-  
427 2672.2008.03870.x

428 Fang, C., Radosevich, M., Fuhrmann, J.J., 2001. Atrazine and phenanthrene degradation in  
429 grass rhizosphere soil. *Soil Biol. Biochem.* 33, 671–678. doi:10.1016/S0038-  
430 0717(00)00216-9

431 Gao, Y., Zhu, L., 2004. Plant uptake, accumulation and translocation of phenanthrene and  
432 pyrene in soils. *Chemosphere* 55, 1169–78. doi:10.1016/j.chemosphere.2004.01.037

433 Günther, T., Dornberger, U., Fritsche, W., 1996. Effects of ryegrass on biodegradation of  
434 hydrocarbons in soil. *Chemosphere* 33, 203–215. doi:10.1016/0045-6535(96)00164-6

435 Hartmann, R., 1996. Polycyclic aromatic hydrocarbons (PAHs) in forest soils: Critical  
436 evaluation of a new analytical procedure. *Int. J. Environ. Anal. Chem.* 62, 161–173.  
437 doi:10.1080/03067319608027062

438 Herrmann, A.M., Ritz, K., Nunan, N., Clode, P.L., Pett-Ridge, J., Kilburn, M.R., Murphy, D.  
439 V., O'Donnell, A.G., Stockdale, E.A., 2007. Nano-scale secondary ion mass spectrometry  
440 - A new analytical tool in biogeochemistry and soil ecology: A review article. *Soil Biol.*

441 Biochem. 39, 1835–1850. doi:10.1016/j.soilbio.2007.03.011

442 Hoppe, P., Cohen, S., Meibom, A., 2013. NanoSIMS: technical aspects and applications in  
443 cosmochemistry and biological geochemistry. *Geostand. Geoanalytical Res.* 37, 111–154.  
444 doi:10.1111/j.1751-908X.2013.00239.x

445 Hwang, S., Cutright, T.J., 2002. Biodegradability of aged pyrene and phenanthrene in a natural  
446 soil. *Chemosphere* 47, 891–899. doi:10.1016/S0045-6535(02)00016-4

447 Joner, E.J., Corgie, S.C., Amellal, N., Leyval, C., 2002. Nutritional constraints to degradation  
448 of polycyclic aromatic hydrocarbons in a simulated rhizosphere. *Soil Biol. Biochem.* 34,  
449 859–864. doi:10.1016/S0038-0717(02)00018-4

450 Joner, E.J., Hirmann, D., Szolar, O.H.J., Todorovic, D., Leyval, C., Loibner, A.P., 2004.  
451 Priming effects on PAH degradation and ecotoxicity during a phytoremediation  
452 experiment. *Environ. Pollut.* 128, 429–35. doi:10.1016/j.envpol.2003.09.005

453 Käcker, T., Haupt, E.T.K., Garms, C., Francke, W., Steinhart, H., 2002. Structural  
454 characterisation of humic acid-bound PAH residues in soil by <sup>13</sup>C-CPMAS-NMR-  
455 spectroscopy: Evidence of covalent bonds. *Chemosphere* 48, 117–131.  
456 doi:10.1016/S0045-6535(02)00082-6

457 Kästner, M., Streibich, S., Beyrer, M., Richnow, H.H., Ka, M., 1999. Formation of bound  
458 residues during microbial degradation of [ <sup>14</sup>C ] anthracene in soil. *Appl. Environ.*  
459 *Microbiol.* 65, 1834–1842. doi:0099-2240/99/\$04.00+0

460 Kipopoulou, A.M., Manoli, E., Samara, C., 1999. Bioconcentration of polycyclic aromatic  
461 hydrocarbons in vegetables grown in an industrial area. *Environ. Pollut.* 106, 369–80.

462 Liste, H.H., Alexander, M., 2000. Plant-promoted pyrene degradation in soil. *Chemosphere* 40,  
463 7–10. doi:10.1016/S0045-6535(99)00216-7

464 Macleod, C.J.A., Semple, K.T., 2003. Sequential extraction of low concentrations of pyrene  
465 and formation of non-extractable residues in sterile and non-sterile soils. *Soil Biol.*

466 Biochem. 35, 1443–1450. doi:10.1016/S0038-0717(03)00238-4

467 Magee, B.R., Lion, L.W., Lemley, A.T., 1991. Transport of dissolved organic macromolecules  
468 and their effect on the transport of phenanthrene in porous media. *Environ. Sci. Technol.*  
469 25, 323–331. doi:10.1021/es00014a017

470 Miya, R.K., Firestone, M.K., 2000. Phenanthrene-degrader community dynamics in  
471 rhizosphere soil from a common annual grass. *J. Environ. Qual.* 29, 584.  
472 doi:10.2134/jeq2000.00472425002900020029x

473 Moore, K.L., Lombi, E., Zhao, F.J., Grovenor, C.R.M., 2012. Elemental imaging at the  
474 nanoscale: NanoSIMS and complementary techniques for element localisation in plants.  
475 *Anal. Bioanal. Chem.* 402, 3263–3273. doi:10.1007/s00216-011-5484-3

476 Northcott, G.L., Jones, K.C., 2001. Partitioning, extractability, and formation of non extractable  
477 PAH residues in soil.2. Effects on compound dissolution behaviour. *Environ. Sci. Technol.*  
478 35, 1111–1117. doi:10.1021/es000072q

479 Pignatello, J.J., Xing, B., 1996. Mechanisms of slow sorption of organic chemicals to natural  
480 particles. *Environ. Sci. Technol.* 30, 1–11. doi:10.1021/es940683g

481 Printz, B., Guerriero, G., Sergeant, K., Audinot, J.-N., Guignard, C., Renaut, J., Lutts, S.,  
482 Hausman, J.-F., 2016. Combining-omics to unravel the impact of copper nutrition on  
483 Alfalfa (*Medicago sativa*) stem metabolism. *Plant Cell Physiol.* 57, 407–22.  
484 doi:10.1093/pcp/pcw001

485 Reilley, K.A., Banks, M.K., Schwab, A.P., 1996. Dissipation of polycyclic aromatic  
486 hydrocarbons in the rhizosphere. *J. Environ. Qual.* 25, 212.  
487 doi:10.2134/jeq1996.00472425002500020002x

488 Remusat, L., Hatton, P., Nico, P.S., Zeller, B., Kleber, M., Derrien, D., 2012. NanoSIMS study  
489 of organic matter associated with soil aggregates: advantages, limitations, and  
490 combination with STXM. *Environ. Sci. Technol.* 46, 3943–3949. doi:10.1021/es203745k

491 Rezek, J., in der Wiesche, C., Mackova, M., Zadrazil, F., Macek, T., 2008. The effect of  
492 ryegrass (*Lolium perenne*) on decrease of PAH content in long term contaminated soil.  
493 *Chemosphere* 70, 1603–8. doi:10.1016/j.chemosphere.2007.08.003

494 Richnow, H.H., Annweiler, E., Koning, M., Lüth, J.C., Stegmann, R., Garms, C., Francke, W.,  
495 Michaelis, W., 2000a. Tracing the transformation of labelled [1-<sup>13</sup>C]phenanthrene in a  
496 soil bioreactor. *Environ. Pollut.* 108, 91–101. doi:10.1016/S0269-7491(99)00205-5

497 Richnow, H.H., Eschenbach, A., Mahro, B., Kästner, M., Annweiler, E., Seifert, R., Michaelis,  
498 W., 1999. Formation of nonextractable soil residues: A stable isotope approach. *Environ.*  
499 *Sci. Technol.* 33, 3761–3767. doi:10.1021/es980927n

500 Richnow, H.H., Eschenbach, A., Mahro, B., Seifert, R., Wehrung, P., Albrecht, P., Michaelis,  
501 W., 1998. The use of <sup>13</sup>C-labelled polycyclic aromatic hydrocarbons for the analysis of  
502 their transformation in soil. *Chemosphere* 36, 2211–2224. doi:10.1016/S0045-  
503 6535(97)10193-X

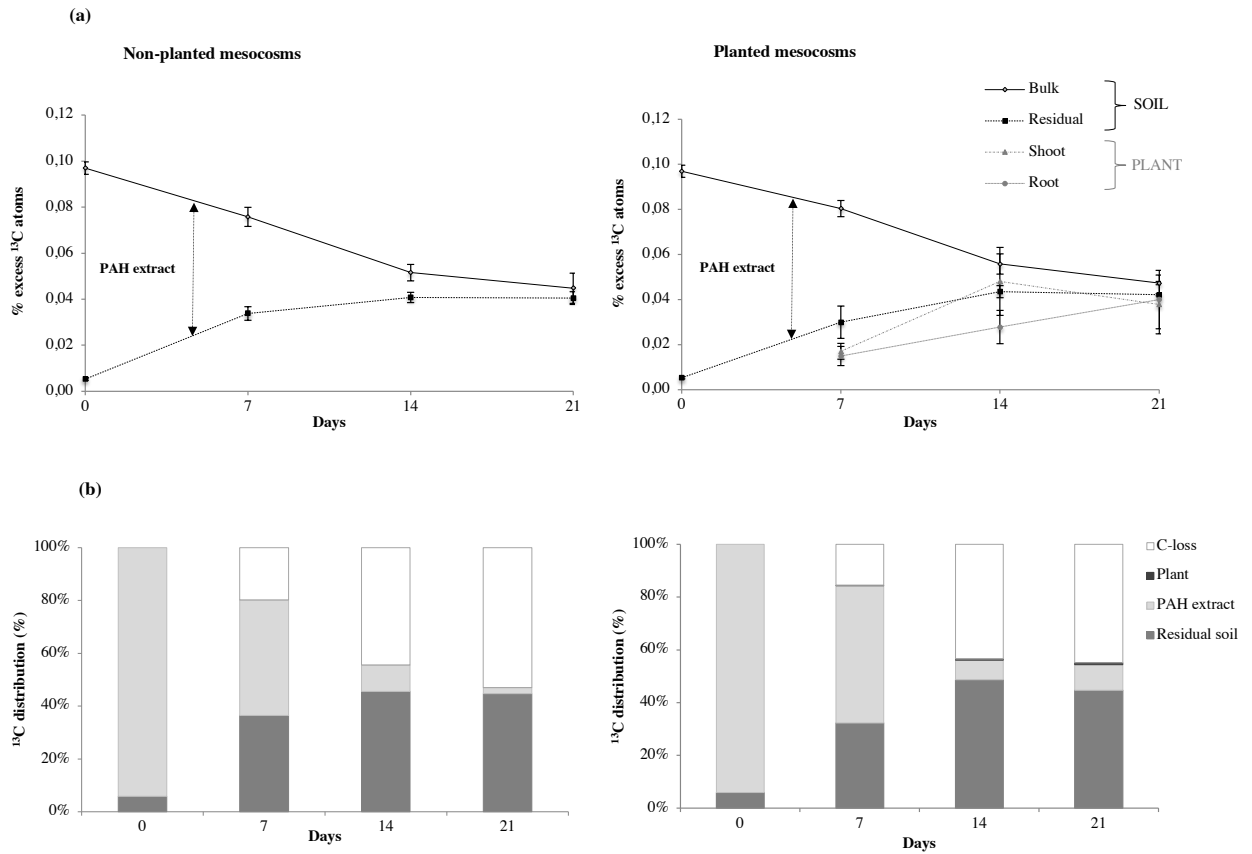
504 Sabaté, J., Viñas, M., Solanas, A.M., 2006. Bioavailability assessment and environmental fate  
505 of polycyclic aromatic hydrocarbons in biostimulated creosote-contaminated soil.  
506 *Chemosphere* 63, 1648–1659. doi:10.1016/j.chemosphere.2005.10.020

507 Schwab, A.P., Banks, M.K., 1994. Biologically mediated dissipation of polyaromatic  
508 hydrocarbons in the root zone. *Am. Chem. Soc.* doi:10.1021/bk-1994-0563.ch012

509 Smith, M.J., Flowers, T.H., Duncan, H.J., Saito, H., 2011. Study of PAH dissipation and  
510 phytoremediation in soils: comparing freshly spiked with weathered soil from a former  
511 coking works. *J. Hazard. Mater.* 192, 1219–1225. doi:10.1016/j.jhazmat.2011.06.033

512 Vidal, A., Remusat, L., Watteau, F., Derenne, S., Quenea, K., 2016. Incorporation of <sup>13</sup>C  
513 labelled shoot residues in *Lumbricus terrestris* casts: A combination of transmission  
514 electron microscopy and nanoscale secondary ion mass spectrometry. *Soil Biol. Biochem.*  
515 93, 8–16. doi:10.1016/j.soilbio.2015.10.018

516 Wilson, S.C., Jones, K.C., 1993. Bioremediation of soil contaminated with polynuclear  
517 aromatic hydrocarbons (PAHs): a review. *Environ. Pollut.* 81, 229–249.  
518 doi:10.1016/0269-7491(93)90206-4  
519  
520



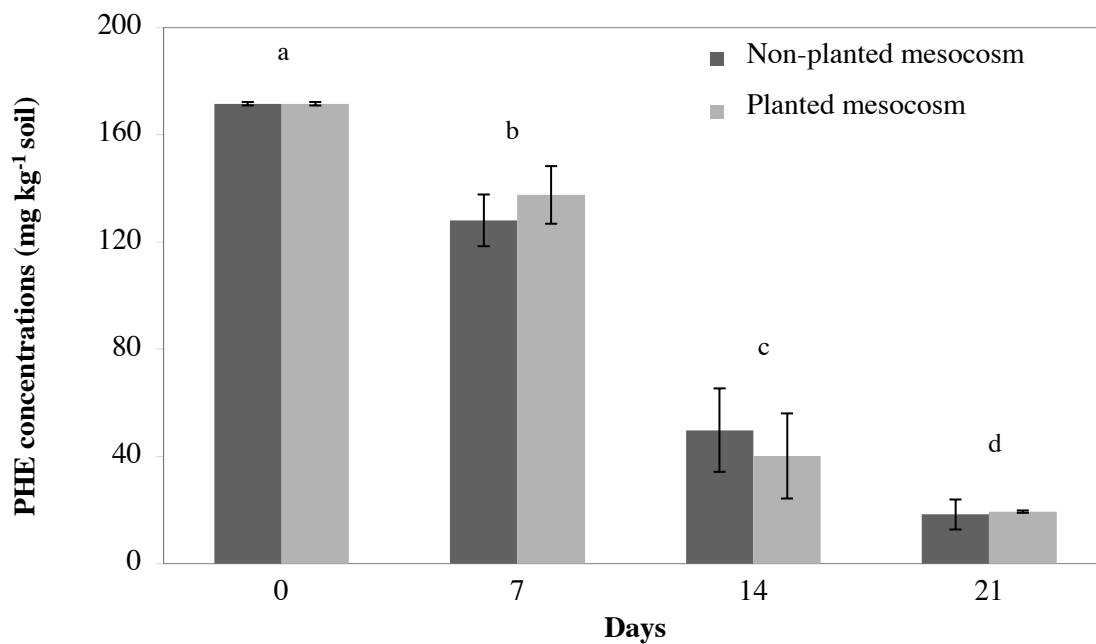
521

522 **Figure 1.** Extractable concentrations of phenanthrene (PHE, mg kg<sup>-1</sup> of soil) in planted and

523 non-planted mesocosms at different time-points over a 21-day period. Means ± SD, n = 4.

524 Different letters indicate significant differences (p<0.05) between the sampling times.

525



526

527 **Figure 2.** <sup>13</sup>C dynamics after <sup>13</sup>C-PHE spiking in non-planted (left) and planted (right)  
 528 mesocosms at different time-points over a 21-day period. **(a)** <sup>13</sup>C enrichment ( $E^{13C}$ , at.%) in the  
 529 plant and soil compartments. Means  $\pm$  SD, n = 4. <sup>13</sup>C enrichment was calculated from  $\delta^{13C}$  data  
 530 obtained by EA-IRMS. **(b)** <sup>13</sup>C distribution in the mesocosm compartments (PAH extract,  
 531 residual soil, plant, and C loss). Results are expressed as percentages of the <sup>13</sup>C-PHE  
 532 concentrations initially added in the soil. The plant compartment gathers root and shoot data.  
 533 PAH extract concentrations were calculated as the difference between bulk and residual soil  
 534 concentrations.

535

536  
537  
538  
539  
540  
541  
542  
543  
544  
545  
546  
547  
548  
549  
550  
551  
552  
553  
554

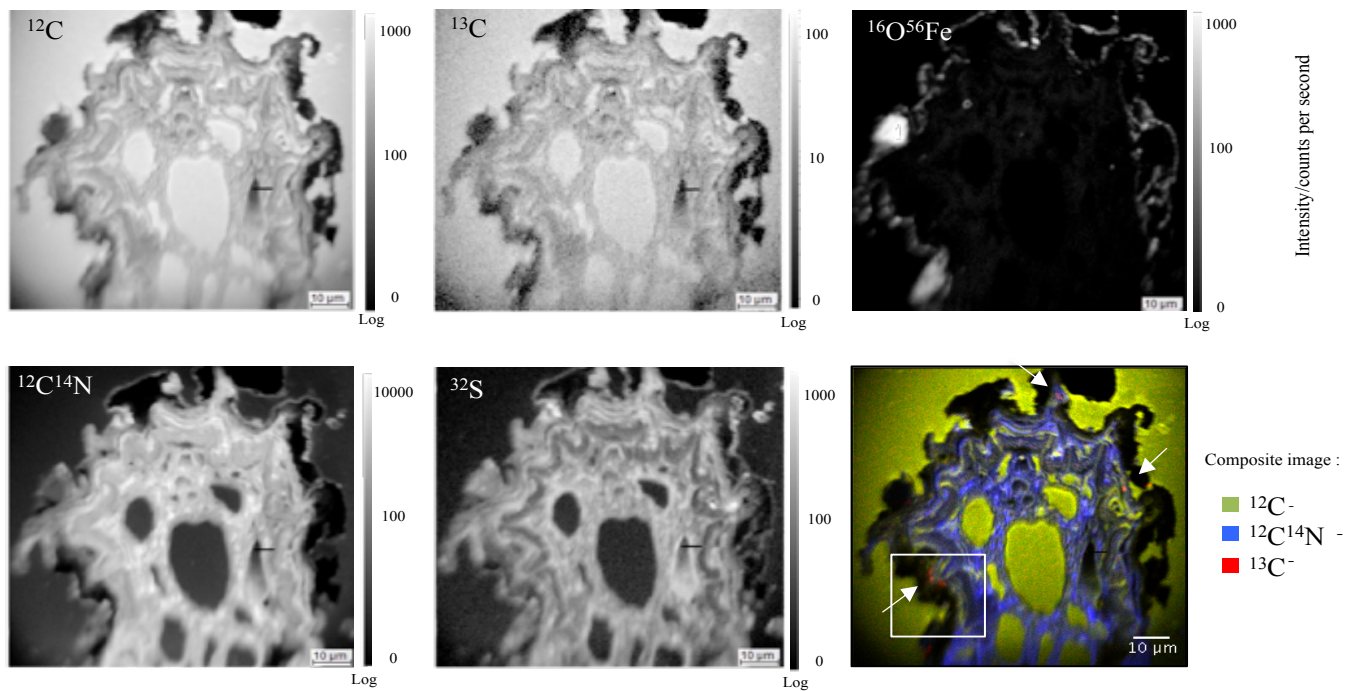
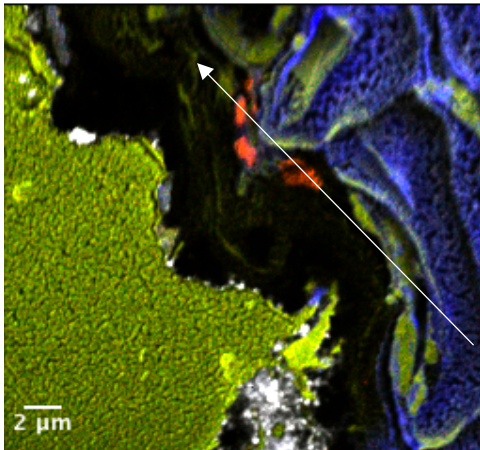


**Figure 3.** NanoSIMS elemental maps of  $^{12}\text{C}^-$ ,  $^{13}\text{C}^-$ ,  $^{12}\text{C}^{14}\text{N}^-$ ,  $^{32}\text{S}^-$  and  $^{56}\text{Fe}^{16}\text{O}^-$  from labeled ryegrass roots after 14 days. The  $90 \times 90\text{-}\mu\text{m}^2$  images are cross views of whole roots with adherent soil particles. A composite image (bottom right) was obtained by overlaying the  $^{12}\text{C}^-$ ,  $^{12}\text{C}^{14}\text{N}^-$  and  $^{13}\text{C}^-$  images. Three areas of interest (bordered in white) with higher  $^{13}\text{C}$  content were identified. NanoSIMS data were analyzed using Winimage software.

555

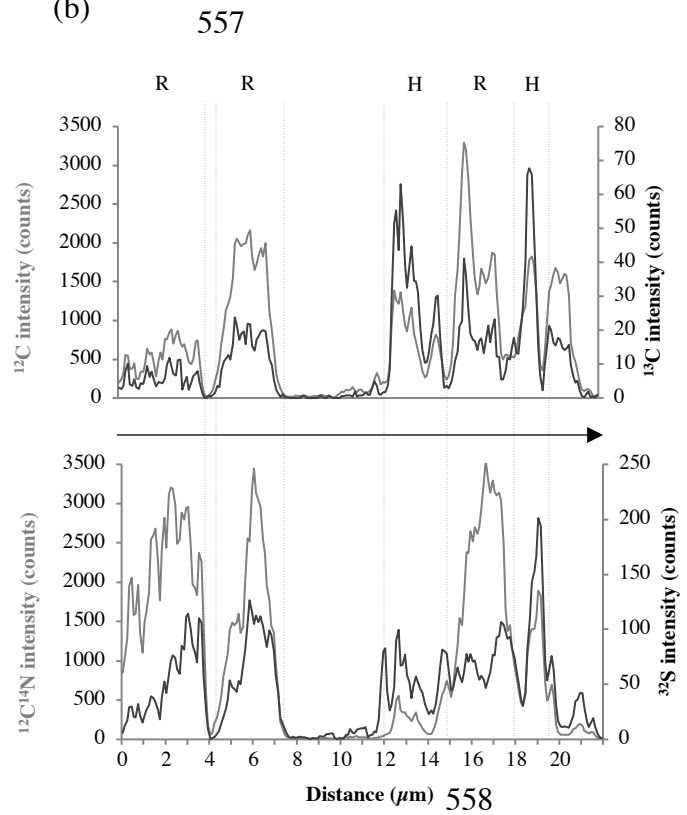
556

(a)



- $^{12}\text{C}^-$
- $^{12}\text{C}^{14}\text{N}^-$
- $^{13}\text{C}^-$
- $^{56}\text{Fe}^{16}\text{O}^-$

(b)



559

560

561 **Figure 4.** NanoSIMS composite image and linescan obtained from root tissue after 14 days.

562 The zone is located inside the white square of Figure 3. (a) Composite 25\*25- $\mu\text{m}^2$  image with

563 hotspots reflecting the  $^{13}\text{C}$ -enrichment (red) obtained by overlaying  $^{12}\text{C}^-$ ,  $^{13}\text{C}^-$ ,  $^{12}\text{C}^{14}\text{N}^-$  and

564  $^{56}\text{Fe}^{16}\text{O}^-$  (white) ion species images. (b) A white segment was drawn through these hotspots

565